Theor Chem Acc (2006) 115: 291–297
DOI 10.1007/s00214-005-0015-y

REGULAR ARTICLE

Shan Xi Tian

Ab initio study of structures and energies of Al_2H_4 and $Al_2H_4^-$

Received: 3 June 2005 / Accepted: 30 August 2005 / Published online: 15 October 2005

Abstract The low-lying isomers of Al_2H_4 and their anions are investigated with the hybrid density functional B3LYP, the coupled-cluster CCSD and CCSD(T) methods, and the electron propagator theory. The positive adiabatic electron affinities 5,798 and 10,112 cm^{-1} are predicted for the neutral C_{2v} and D_{2d} symmetric isomers, respectively. The D_{2h} symmetric anion is more stable by 852 cm^{-1} than the C_{2v} symmetric anion. The photodetachment spectra for $Al_2H_4^-$ anions at the C_{2v} and D_{2h} symmetries are simulated on the basis of the Franck–Condon factor calculations, indicating a reasonable way to study the transition state of the intramolecular torsion process.

Keywords Electron Affinity · Isomer · Dialane(4) · Franck–Condon factor · Transition state

1 Introduction

Dialanes regarding Al_2H_2 [1], Al_2H_4 [2] and Al_2H_6 [1,3] are recently studied because of their novel electron-deficient bonding characteristics. As far as dialane(4) Al_2H_4, the salt-like isomers (**1** and **2** as shown in Fig. 1) are predicted to be the most stable on the basis of ab initio calculations [4]. Isomer **3** is a little less stable than the former two. Conformers **4** and **T12** (corresponding respectively to **5**, **3** of Ref. [4]) are the transition structures, but no information of their relationship to the stable isomers have been known. On the other hand, the extremely interesting bonding features, namely the three-center two-electron (3c-2e) and two-center one-electron (2c-1e) bonds, are found in the anions of dialane(6) Al_2H_6 [5,6]. To our best knowledge, no studies of the isomerism of dialane(4) and the radical anions have been reported. We will study the structural and energetic properties of Al_2H_4 and $Al_2H_4^-$, several points will be focused on in this work:

1. Although **1** and **2** isomers are thought to be the salt-like conformers as Al^+ combined with AlH_4^- [4], the multiple 3c-2e bonding may be the real factor to stabilize these two conformers.
2. The transition structures between the most stable isomers will be located, and the energetic barriers will be predicted.
3. Electron attachment may break the 3c-2e bond in dialane [6], what will happen in the $Al_2H_4^-$ anions? The bonding characteristics of the $Al_2H_4^-$ anions will be analyzed.
4. The photoelectron detachment spectra of these anions will be theoretically simulated, hopefully providing assignments for the future experiments.

2 Theoretical methods

Ab initio calculations were performed with Gaussian 98 program [7]. As pointed out in our previous work [6,8], electron correlation effects were essential to predict energies and geometries in good agreement with the experimental data; moreover, the polarization functions on hydrogen atoms improved the description of the bridging hydrogen atoms (H_b or μ-H). Thereby, the hybrid density functional B3LYP method [9,10], the coupled-cluster CCSD theory [11] and the Dunning's correlation consistent basis set aug-cc-pvDZ [12] were used in the geometrical optimizations and harmonic vibrational frequency calculations. The chemical bond characteristics were analyzed by natural bond orbital (NBO) theory [13]. The NBO analyses transferred the delocalized molecular orbitals (MOs) into the localized ones that were closely tied to chemical bond concepts. 3c-2e bond search was activated with 3CBOND keyword [14], using the Hartree-Fock (HF) canonical wave functions over the CCSD optimized geometries. The second-order perturbation interaction energies and hybrid compositions, occupancies and energies of

S. X. Tian
Hefei National Laboratory for Physical Sciences at Microscale, Laboratory of Bond Selective Chemistry, and Department of Chemical Physics, University of Science and Technology of China, Hefei, Anhui 230026, People's Republic of China
E-mail: sxtian@ustc.edu.cn
Tel.: +86-551-3607736
Fax: +86-551-3602969

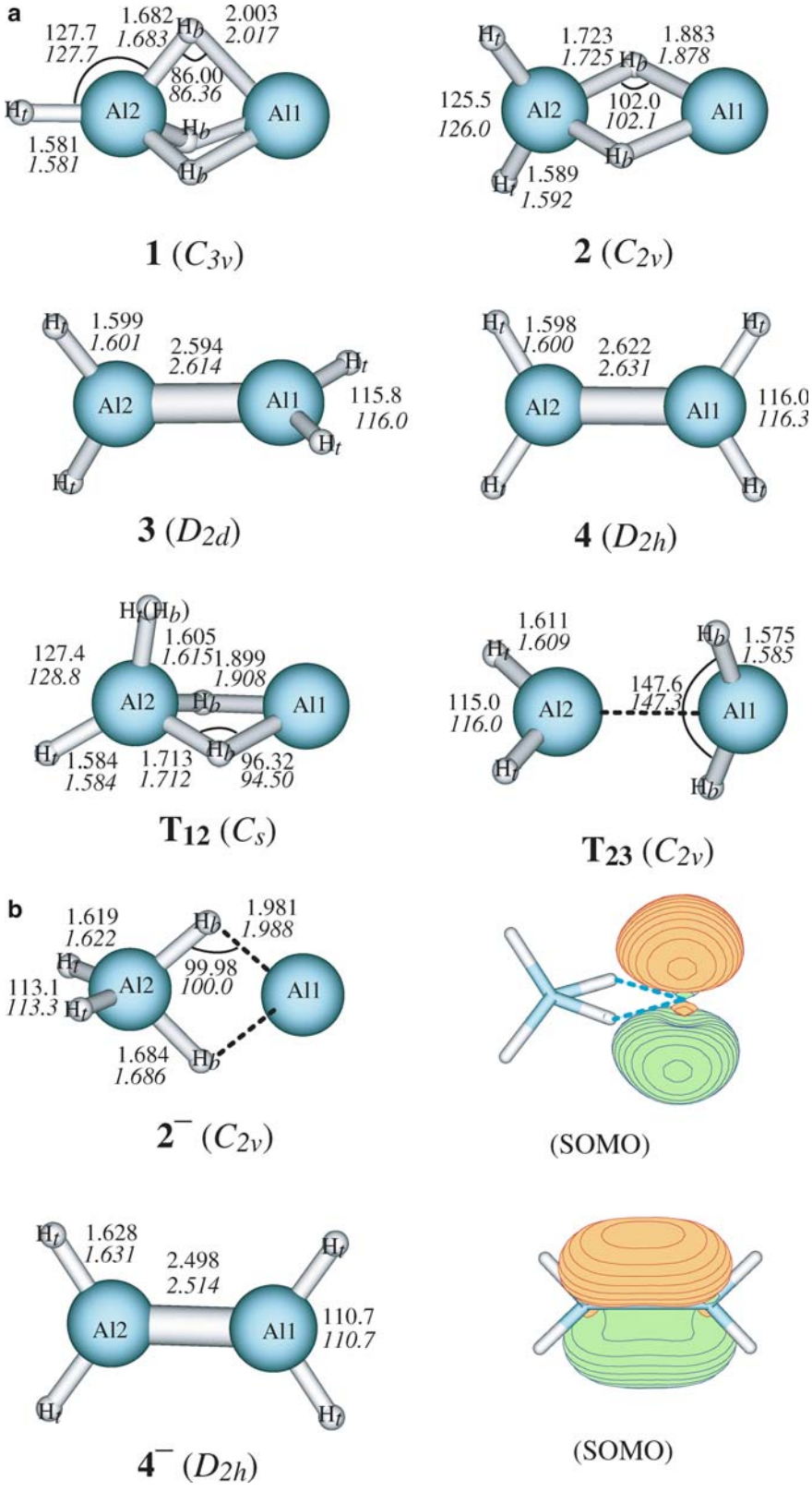

Fig. 1 Optimized molecular structures: B3LYP/aug-cc-pvDZ (*roman*) and CCSD/aug-cc-pvDZ (*italic*)

the 3c-2e bonds were calculated. The transition structures **T12** (between **1** and **2** isomers) and **T23** (between **2** and **3** isomers) were located by the synchronous transit-guided quasi-Newton (STQN) method [15], and the energetic extrapolated CCSD(T) [11, 16] calculations were carried out over the CCSD optimized geometries.

To include electron correlation and orbital relaxation effects in the electron attachments to the neutral and photodetachment of the anions, the partial third-order quasiparticle approximation (P3) of the electron propagator theory [17] was used to calculate the vertical electron affinities (EA_vs) of the neutral and the vertical detachment energies (VDEs) of the anions. The adiabatic electron affinity (EA_a), EA_v, and VDE values were also calculated at the B3LYP, CCSD, and CCSD(T) levels,

$$EA_a = E(M_{\text{neutral}}) - E(M^-_{\text{anion}})$$
$$EA_v = E(M_{\text{neutral}}) - E(M^-_{\text{neutral}})$$

and

$$VDE = E(M_{\text{anion}}) - E(M^-_{\text{anion}})$$

where the zero-point vibrational energy (ZPVE) corrections were considered in the EA_a calculations. The respective optimized geometries were used in the total energy (E) calculations for EA_a values, while only the neutral or anionic geometries were used in the EA_v or VDE calculations.

3 Results and discussion

As shown in Fig. 1a, the low-lying neutral isomers **1**, **2**, **3**, **4** and **T12** are similar to those optimized at HF/6-31G* level of theory [4]. The geometrical parameters distinctly differ from the HF/6-31G* ones, not only due to the electron correlation effect but also the larger flexible basis set used in this work. In general, the B3LYP optimized parameters are close to the CCSD ones. **4** corresponds to a transition state of the intramolecular AlH_2 torsion process of **3**; **T12** corresponds to a transition state between **1** and **2** isomers; The transition state between **2** and **3** isomers is **T23** shown in Fig. 1a. One 3c-2e bond (as discussed in the following text) is broken for **1** → **2**; while double 3c-2e bonds are broken for **2** → **3**. The optimization of the anionic structure within C_{3v} symmetry limitation failed, finally leading to $\mathbf{2}^-(C_{2v})$. The optimization of the anionic structures at the D_{2d} and D_{2h} symmetries only produced the stable anionic $\mathbf{4}^-(D_{2h})$. The anionic species are shown in Fig. 1b, and the electron densities of the single occupied MOs (SOMOs) have been plotted with a contour value ±0.05. The broken lines shown in $\mathbf{2}^-(C_{2v})$ suggest that there might be no covalent bonds between H_b and Al_1 atoms, and the extra electron mainly occupies at 3*p* orbital of Al_1 atom. The bond length between Al_1 and Al_2 is significantly shortened by ca. 0.1 Å in $\mathbf{4}^-(D_{2h})$ with respect to that in $\mathbf{4}(D_{2h})$ or $\mathbf{3}(D_{2d})$. The electron density plots indicate that the extra electron occupies on a π orbital, namely, a two-center three-electron (2c-3e) bond Al.·.Al can be formed in $\mathbf{4}^-$. However, the 2c-3e bonds O.·.O, N.·.N, S.·.S, P.·.P and Si.·.Si

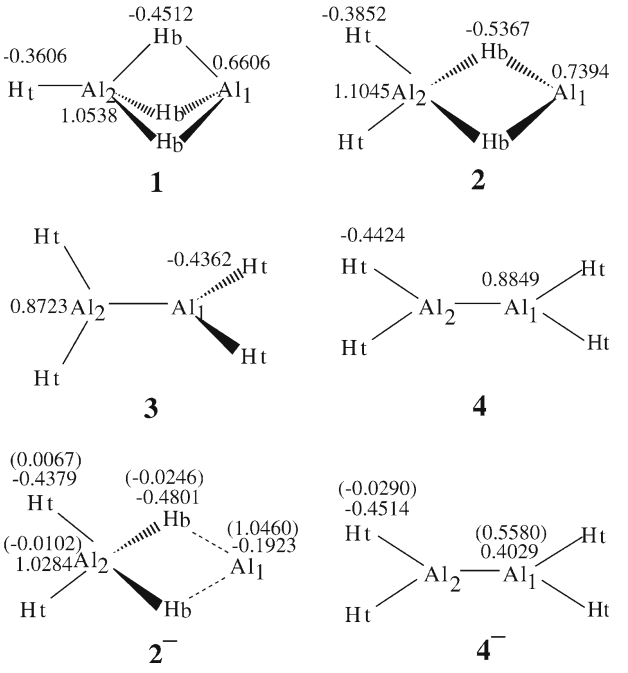

Fig. 2 Natural atomic populations obtained over the CCSD/aug-cc-pvDZ optimized geometries. The values in the *parentheses* are the Mulliken atomic spin densities for the anions

in the anionic radicals were found to be weaker than the covalent two-electron bonds due to the extra electron occupied on the anti-bond orbitals [18].

Natural charge population on each atom is presented in Fig. 2. Both the terminal H (H_t) and H_b atoms are negatively charged. In particular, the electronic repulsive interactions of H_t atoms cannot simply explain that **3** is more energetically favorable than **4**. Mulliken atomic spin density on each atom in the anion is also shown in the parenthesis, indicating that the extra electron is mainly on Al_1 atom in $\mathbf{2}^-$ or two Al atoms in $\mathbf{4}^-$. This is consistent with the electron density plots in Fig. 1b.

Harmonic vibrational frequencies and infrared (IR) intensities of the stable conformers are summarized in Table 1. Single-imaginary frequencies have been predicted to be *i*135 (*i*115) cm^{-1}, *i*151 (*i*165) cm^{-1} and *i*1011 (*i*1029) cm^{-1} for **4**, **T12**, and **T23**, respectively, at the B3LYP (or CCSD) level of theory. The experimental data from Ref. [1] are tentatively assigned and compared with the present results. It is noted that the experimental datum 924 cm^{-1} was assigned to an asymmetric stretching of the Al(μ-H)$_3$Al bonds along the Al-Al axis [1], while here it corresponds to a symmetric stretching of the Al(μ-H)$_3$Al bonds perpendicular to the Al-Al axis according to the CCSD calculations. There are remarkable frequency shifts of $\mathbf{2}^-$ with respect to **2** although they have similar geometries. Until now, no experimental IR spectra of above anions are reported. The IR fingerprints may be ca. 990 cm^{-1} for $\mathbf{2}^-$ and ca. 1,700 cm^{-1} for $\mathbf{4}^-$. In fact, $\mathbf{4}^-$ is more stable by 852 cm^{-1} than $\mathbf{2}^-$ at the CCSD(T)//CCSD level. The transition between $\mathbf{2}^-$ and $\mathbf{4}^-$ is energetically unfavorable because of their distinctly different bonding structures as discussed below.

Table 1 Harmonic vibrational frequencies (cm^{-1}) and infrared intensities (km mol^{-1}) of the stable conformers

Molecule	Method	Frequency (Symmetry, Intensity)
1(C_{3v})	B3LYP	368(e″,4×2), 796(e″,550×2), 879(e″,73×2), 1545(e″,80×2); 400(a_1,82), 902(a_1,819), 1666(a_1,83), 1935(a_1,308)
	CCSD	335(e″,7×2), 806(e″,326×2), 892(e″,42×2), 1559(e″,41×2); 398(a_1,106), 942(a_1,1045), 1691(a_1,123), 1950(a_1,257)
	Exptl.[a]	844.1(e″),[b] 924(a_1)[c]
2(C_{2v})	B3LYP	325(a_1,41), 720(a_1,332), 1161(a_1,1056), 1549(a_1,425), 1890(a_1,122); 611(a_2,0); 498(b_1,26), 1055(b_1,425), 1321(b_1,2); 120(b_2,19), 798(b_2,106), 1903(b_2,217)
	CCSD	330(a_1,46), 729(a_1,355), 1206(a_1,1230), 1568(a_1,518), 1899(a_1,109); 664(a_2,0); 496(b_1,24), 1068(b_1,415), 1325(b_1,6); 130(b_2,22), 805(b_2,107), 1911(b_2,218)
	Exptl.[a]	1156.1(a_1)[d]
3(D_{2d})	B3LYP	229(e,67×2), 548(e,69×2), 1866(e,250×2); 337(a_1,0), 808(a_1,0), 1869(a_1,0); 137(b_1,0); 747(b_2,682), 1847(b_2,380)
	CCSD	318(e,73×2), 557(e,77×2), 1872(e,255×2); 348(a_1,0), 815(a_1,0), 1876(a_1,0); 110(b_1,0); 755(b_2,735), 1855(b_2,386)
	Exptl.[a]	747(b_2), 1825.5(b_2), 1835.8(e),[e] 1838.4(e),[e]
2$^-$(C_{2v})	B3LYP	278(a_1,23), 768(a_1,580), 973(a_1,870), 1627(a_1,406), 1772(a_1,475); 581(a_2,0); 246(b_1,14), 638(b_1,45), 1744(b_1,297); 450(b_2,2), 891(b_2,321), 1461(b_2,10)
	CCSD	277(a_1,37), 773(a_1,548), 993(a_1,1059), 1641(a_1,491), 1782(a_1,394); 600(a_2,0); 252(b_1,4), 656(b_1,59), 1754(b_1,309); 429(b_2,0), 899(b_2,389), 1471(b_2,9).
4$^-$(D_{2h})	B3LYP	378(a_g,0), 799(a_g,0), 1751(a_g,0); 299(a_u,0); 736(b_{1u},341), 1719(b_{1u},721); 310(b_{2g},0); 283(b_{2u},53), 1723(b_{2u},909); 467(b_{3g},0), 1715(b_{3g},0); 448(b_{3u},37)
	CCSD	387(a_g,0), 803(a_g,0), 1759(a_g,0); 310(a_u,0); 737(b_{1u},324), 1728(b_{1u},775); 335(b_{2g},0); 287(b_{2u},56), 1730(b_{2u},905); 468(b_{3g},0), 1722(b_{3g},0); 466(b_{3u},37)

[a] From Ref. [1], the symmetry assigned to the experimental data is given in this work
[b] Two doubly degenerate e″ vibrational models are perhaps involved
[c] Symmetric stretching of the Al(μ-H)$_3$Al bonds perpendicular to the Al–Al axis
[d] Assigned to the bridge stretching model of Al_2H_2 in Ref. [1]
[e] Split vibrations due to the matrix effect (see Ref. [1])

Table 2 Relative energies (kcal mol^{-1}) with respect to the neutral **1**(C_{3v})

	1(C_{3v})	**2**(C_{2v})	**3**(D_{2d})	**4**(D_{2h})	$\mathbf{T}_{12}(C_s)$	$\mathbf{T}_{23}(C_{2v})$[a]
B3LYP	0.00	1.89	10.51	11.98	2.42	54.32
B3LYP+ZPVE[b]	0.00	1.78	9.22	10.65	2.23	51.63
CCSD	0.00	0.46	9.79	10.81	1.38	58.83
CCSD+ZPVE[b]	0.00	0.41	8.49	9.46	1.18	55.74
CCSD(T)[c]	0.00	1.17	11.06	12.13	1.77	57.36

[a] Relative to **2**(C_{2v})
[b] The zero-point-vibrational energy corrections are included
[c] Over the CCSD/aug-cc-pvDZ optimized geometries, and without the zero-point-vibrational energy corrections

Table 3 Second-order perturbation interaction energies (kcal mol^{-1}) for the staggered (D_{2d}) and eclipsed (D_{2h}) conformers[a]

	Neutral		Difference	Anion		Difference
	3(D_{2d})	**4**(D_{2h})	Staggered – Eclipsed	D_{2d}^b	**4**$^-$(D_{2h})	Staggered – Eclipsed
All vicinal[c]	0.00	2.72	−2.72	0.00	4.88	−4.88
All geminal[d]	69.88	74.68	−4.80	49.44	41.68	7.76
Others[e]	10.16	8.08	−2.08	43.89	7.02	36.87
Total	80.04	85.48	−5.44	93.33	53.58	39.75

[a] Over the CCSD/aug-cc-pvDZ optimized geometries
[b] Optimized geometrical parameters: Al–Al = 2.58 Å, Al–H_t = 1.63 Å, $\angle H_tAlH_t = 125^\circ$
[c] Only interactions involving adjacent atomic centers, none of which is in common
[d] Only interactions involving at least one common atomic center
[e] Only interactions involving Rydberg, core electrons or lone pair

Table 2 lists the relative energies of the neutral isomers with respect to **1**. The stability order is in agreement with the previous conclusion [4]: **1** > **2** > **3** > **4**. To break one of the triple 3c-2e bonds may cost ca. 2 kcal mol^{-1}; while to break two 3c-2e bonds together will cost more than ca. 40 kcal mol^{-1}, estimated from the relative energies of **T12** and **T23**.

Now we focus on the staggered (D_{2d}) or eclipsed (D_{2h}) preference of Al_2H_4. Since the hyperconjugation in the anions is a major structural determinant [19,20], these intramolecular interactions are discussed here. Table 3 lists the vicinal, geminal, and other components of the second-order perturbation interactions energy. The more stable conformers exhibit the smaller interaction energies, thereby the anion prefers D_{2h} symmetry and the neutral is of D_{2d} symmetry. Al–H/Al–H* interactions are the main contributions of the vicinal part, but they disappear in the D_{2d} symmetric

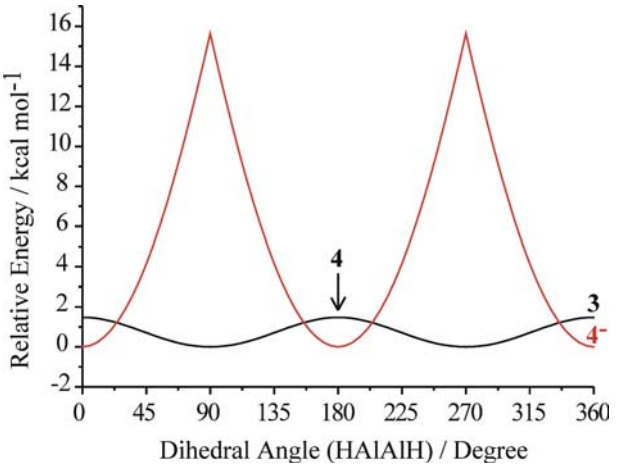

Fig. 3 Torsional potential curves of the neutral **3**(D_{2d}) or **4**(D_{2h}) and the anion $\mathbf{4}^-$(D_{2h}). Zero energy points are arbitrarily taken at 90 and 0° for the neutral and anion, respectively

conformers and only very small amount is owing to them in the D_{2h}symmetric ones. The strong Al–H/Al(3p)* interactions (12.08 kcal mol^{-1} included in the other hyperconjugations) in the D_{2d} anion suggest that the rotation of AlH_2 group needs a considerable energy. Torsional potential curves of the neutral and anion with the geometrical relaxation were calculated at the B3LYP level and shown in Fig. 3. It is clear that **4** is the torsional transition state of **3**(D_{2d}), while the anion at the D_{2d} symmetry may correspond to a higher-order saddle point on the anionic potential surface. The latter may be due to the π bond (the SOMO of $\mathbf{4}^-$) breaking during the torsion.

In contrast to the previous NBO analyses [4], the typical 3c-2e bonds are observed in **1** and **2** isomers. Table 4 summarizes the hybrid composition, occupancy and energy level of each important chemical bond. However, more p hybrids are predicted on Al_1 atom in **1** or **2**, due to no terminal H atoms combined with it. The doubly occupied Al–Al bond in **4** exhibits the small occupancy and higher energy level because of its less stability with respect to **3**. No covalent chemical bond is predicted between two Al atoms and no 3c-2e bonds exist in $\mathbf{2}^-$. In the 2c-3e Al.·Al bond of $\mathbf{4}^-$, the SOMO occupies at the higher-level π orbital, while the other two electrons form a σ bond.

The CCSD and CCSD(T) methods failed in the EA_v calculations of **1**(C_{3v}). $^2A_1$ state was reached at the B3LYP level while ^2E state was predicted at the P3 level, indicating the significant effects of the electronic relaxations involved in the latter method. Only is the vertical electron attachment to **1**(C_{3v}) endothermic. The vertical attachments to form the other two stable anions are exothermic with 3,000 $\sim$ 6,000 cm^{-1}. In Table 5, the distinct differences of EA_v, EA_a and VDE values can be found among the various theoretical methods. The VDEs for $\mathbf{2}^-$ and $\mathbf{4}^-$ are 6,735 and

Table 4 Hybrids, occupancies and energy levels of some selected natural bonds over the CCSD/aug-cc-pvDZ optimized geometries

		Hybrid Composition	Occupancy	Energy(au)
1(C_{3v})[a]	$Al_1-H_b-Al_2$	$0.2474(sp^{26.68}\ d^{0.50})Al_1+0.4554(sp^{4.44}\ d^{0.06})Al_2+0.8552(sp^{0.01})H_b$	1.9731	−0.5103
2(C_{2v})[a]	$Al_1-H_b-Al_2$	$0.2581(sp^{20.10}\ d^{0.50})Al_1+0.3973(sp^{5.98}\ d^{0.16})Al_2+0.8806(sp^{0.01})H_b$	1.9733	−0.5262
3(D_{2d})	Al_1-Al_2	$0.7071(sp^{1.49}\ d^{0.02})Al\times2$	1.9149	−0.4143
4(D_{2h})	Al_1-Al_2	$0.7071(sp^{1.99}\ d^{0.02})Al\times2$	1.9052	−0.4098
$\mathbf{2}^-$(C_{2v})[b]	Al_2-H_b	α: $0.4553(sp^{3.69}\ d^{0.05})Al_2+0.8904(sp^{0.01})H_b$	0.9275	−0.3081
		β: $0.4536(sp^{3.77}\ d^{0.05})Al_2+0.8912(sp^{0.01})H_b$	0.9291	−0.3077
$\mathbf{4}^-$(D_{2h})	Al_1-Al_2	α: $0.7071(sp^{1.00}\ d^{0.01})Al\times2$	0.9967	−0.0482
		α: $0.7071(sp^{1.51}\ d^{0.03})Al\times2$	0.9713	−0.2832
		β: $0.7071(sp^{1.58}\ d^{0.03})Al\times2$	0.9804	−0.2617

[a] No bond is formed between two aluminum atoms
[b] No three-center bonds Al_1-H_b-Al_2 are formed

Table 5 Vertical and adiabatic electron affinities (EA_v and EA_a in cm^{-1}) and the vertical detachment energies (VDEs in cm^{-1})

	1(C_{3v})		**2**(C_{2v})		**3**(D_{2d})		VDE	
	EA_v	EA_a^a	EA_v	EA_a^a	EA_v	EA_a^b	$\mathbf{2}^-$(C_{2v})	$\mathbf{4}^-$(D_{2h})
B3LYP[c]	−2689[e]	6,189	5,728	6,813	4,787	11,356	7,323	12,336
CCSD[c]	–[f]	5,651	4,602	5,796	3,577	9,955	6,383	10,813
CCSD(T)[d]	–[f]	5,391	4,940	5,798	3,955	10,112	6,684	11,236
P3[d]	−5097[g]		4,791		2,839		6,735	11,106

[a] Corresponding to the anion $\mathbf{2}^-$ (C_{2v})
[b] Corresponding to the anion $\mathbf{4}^-$ (D_{2h})
[c] Over the respective optimized geometries and including the zero-point-vibrational energy corrections in the EA_a calculations
[d] Over the CCSD/aug-cc-pvDZ optimized geometries and without the zero-point-vibrational energy corrections
[e] Corresponding to $^2A_1$ state
[f] Failed in convergence
[g] Corresponding to ^{2} E state

Table 6 Theoretical values of Franck-Condon (FC) factors and transition energies (TE in cm^{-1}) in the photoelectron spectra of $\mathbf{2}^-(C_{2v})$ and $\mathbf{4}^-(D_{2h})$ isomers

Assignment[a]	TE[b]	FC(≥0.01)	Assignment[a]	TE[b]	FC(≥0.05)[c]
$\mathbf{2}^-(C_{2v})\rightarrow\mathbf{2}(C_{2v})$			$\mathbf{4}^-(D_{2h})\rightarrow\mathbf{4}(D_{2h})$		
0_0^0	5796	1.00	0_0^0	10295	1.00
2_0^1	6072	0.32	4_0^1	10683	0.09
1_0^2	6300	0.04	2_0^2	10915	0.11
6_0^1	6569	0.20	8_0^1	11098	0.53
$1_0^2 2_0^1$	6577	0.01	$4_0^1 8_0^1$	11486	0.05
$1_0^1 5_0^1$	6764	0.02	$2_0^2 8_0^1$	11718	0.06
8_0^1	6788	0.20	8_0^2	11901	0.14
$2_0^1 6_0^1$	6846	0.12	12_0^1	12055	0.87
$2_0^2 6_0^1$	7123	0.01	$4_0^1 12_0^1$	12442	0.07
$3_0^1 7_0^1$	7124	0.01	$2_0^2 12_0^1$	12675	0.09
$2_0^2 8_0^1$	7342	0.01	$8_0^1 12_0^1$	12858	0.47
6_0^2	7342	0.03	$2_0^2 8_0^1 12_0^1$	13478	0.05
$6_0^1 8_0^1$	7561	0.04	$8_0^2 12_0^1$	13661	0.13
12_0^1	7578	0.01	12_0^2	13814	0.35
$2_0^1 6_0^2$	7619	0.02	$8_0^1 12_0^2$	14617	0.19
8_0^2	7781	0.02	$8_0^2 12_0^2$	15420	0.05
$1_0^1 11_0^1$	7802	0.02	12_0^3	15574	0.08

[a] Vibrational models are numbered from the small to the large for $\mathbf{2}^-(C_{2v})$ and $\mathbf{4}^-(D_{2h})$ (see Table 1)
[b] The CCSD/aug-cc-pvDZ geometries and harmonic frequencies are used in the calculations
[c] In Fig. 4, the FC ≥0.01 are included

11,106 cm^{-1}, corresponding to the $\mathbf{2}^-(^2B_1) \rightarrow {}^1A_1$ and $\mathbf{4}^-(^2B_{3u}) \rightarrow {}^1A_g$ transitions, respectively.

To simulate the photodetachment electron spectra, the Franck-Condon factors for the $\mathbf{2}^-(^2B_1) \rightarrow \mathbf{2}(^1A_1)$ and $\mathbf{4}^-(^2B_{3u}) \rightarrow \mathbf{4}(^1A_g)$ transitions were calculated using the CCSD geometrical Hessians and the respective equilibrium geometries of the neutral and anion. The theoretical details can be found in Ref. [21]. The positions of the 0–0 transitions, 5,796 and 10,295 cm^{-1}, were determined from the differences in the CCSD energies of the neutral and anionic species and corrected for the differences of the ZPVEs. The values of Franck–Condon factors reported in Table 6 indicate that the first (b_2), second(a_1), third(b_1), fifth(b_2), sixth(a_1), seventh(b_1), eighth(a_1), eleventh(a_1) and twelfth(b_2) will contribute to the vibrational structure in the photoelectron spectrum of the $\mathbf{2}^-(^2B_1) \rightarrow \mathbf{2}(^1A_1)$ transition; while there are more vibrational modes contributed to the spectrum of the $\mathbf{4}^-(^2B_{3u}) \rightarrow \mathbf{4}(^1A_g)$ transition. The calculated Franck–Condon factors for these two transitions were convoluted with Gaussian lineshapes (FWHM = 100 cm^{-1}) and the resulting theoretical spectra are shown in Fig. 4. Here it is noted that **4** is the transition state of the intramolecular torsion process of **3**, the spectrum of the $\mathbf{4}^-(^2B_{3u}) \rightarrow \mathbf{4}(^1A_g)$ transition could be used to study this intramolecular process (see Fig. 3). The stronger peaks can be recognized from Table 6. The previous transition state spectroscopy only focused on the transition states of the intermolecular reactions [22–24], no studies on the transition state of the intramolecular process are reported. If the anionic intermediates in the intramolecular processes such as torsional isomerism and proton-tranfer tautomerism are energetically stable, the photoelectron spectroscopy will again be a promising way to study these states directly.

4 Conclusion

Ab initio methods regarding B3LYP, CCSD and CCSD(T), and the P3 electron propagator theory have been used in the studies of Al_2H_4 and $Al_2H_4^-$. Multiple 3c-2e bonds are found in the $\mathbf{1}(C_{3v})$ and $\mathbf{2}(C_{2v})$ isomers, while ionic conformer $Al^- \cdot\cdot\cdot AlH_4$ is found for $\mathbf{2}^-(C_{2v})$ and 2c-3e bond is formed in $\mathbf{4}^-(D_{2h})$. $\mathbf{1}(C_{3v})$ and $\mathbf{4}^-(D_{2h})$ may correspond to the global minima on the neutral and anionic potential surfaces, respectively. The positive adiabatic electron affinities 5,798 and 10,112 cm^{-1} are predicted for the neutral $\mathbf{2}(C_{2v})$ and $\mathbf{3}(D_{2d})$ isomers, respectively. The $\mathbf{4}^-(D_{2h})$ anion is 852 cm^{-1} more stable than $\mathbf{2}^-(C_{2v})$ anion. The photodetachment spectra for $Al_2H_4^-$ are simulated on the basis of the Franck–Condon factor calculations, in particular, the $\mathbf{4}^-(^2B_{3u}) \rightarrow \mathbf{4}(^1A_g)$ transition indicates a reasonable way to study the transition state of the intramolecular torsion process.

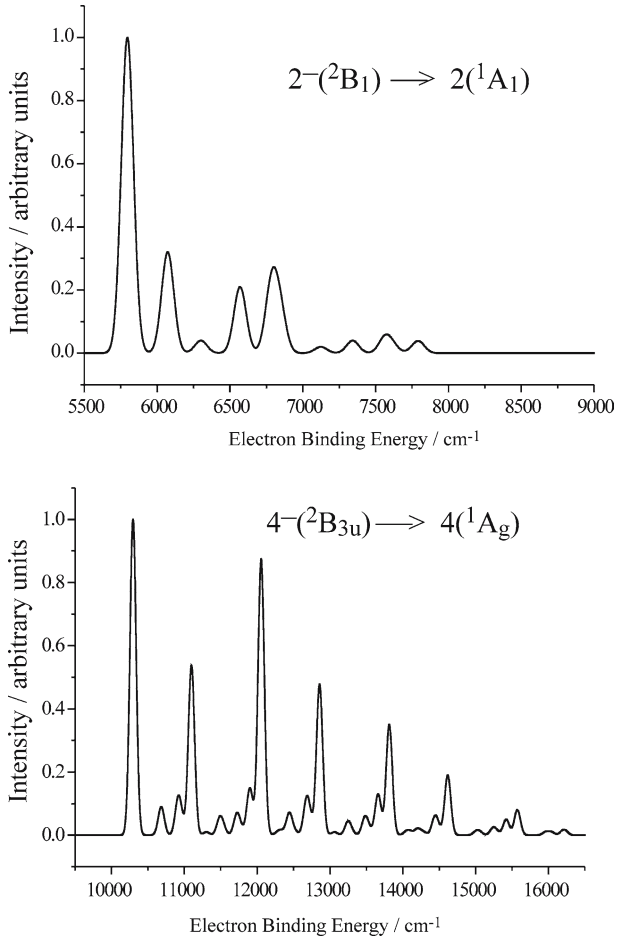

Fig. 4 Theoretical photodetachment electron spectra of $\mathbf{2}^-(C_{2v})$ and $\mathbf{4}^-(D_{2h})$, based on the calculated Franck–Condon factors

References

1. Wang X, Andrews L, Tam S, DeRose ME, Fajardo M (2003) J Am Chem Soc 125:9218
2. Andrews L, Wang X (2003) Science 299:2049
3. Andrews L, Wang X (2004) J Phys Chem A 108:4202
4. Lammertsma K, Guner OF, Drewes RM, Reed AE, Schleyer PvR (1989) Inorg Chem 28:313
5. Rao BK, Jena P, Burkart S, Gantefor G, Seifert G (2001) Phys Rev Lett 86:692
6. Tian SX (2005) J Phys Chem A 109:4428
7. Frisch MJ, et al (1988) Gaussian 98, Revision A.1. Gaussian Inc., Pittsburgh
8. Tian SX (2005) J Phys Chem A 109:5471
9. Becke AD (1993) J Chem Phys 98:5648
10. Lee C, Yang W, Parr RG (1988) Phys Rev B 37:785
11. Scuseria GE, Schaefer HF (1989) J Chem Phys 90:3700
12. Dunning TH Jr.(1989) J Chem Phys 90:1007
13. Reed A, Curtiss LA, Weinhold F (1988) Chem Rev 88:899
14. NBO Version 3.1, Glendening ED, Reed AE, Carpenter JE, Weinhold F (1990)
15. Peng C, Ayala PY, Schlegel HB, Frisch MJ (1996) J Comp Chem 17:49
16. Pople JA, Head-Gordon M, Raghavachari K (1987) J Chem Phys 87:5968
17. Ortiz JV (1996) J Chem Phys 104:7599
18. Braida B, Thogerson L, Wu W, Hiberty PC (2002) J Am Chem Soc 124:11781
19. Hoffmann R, Radom L, Pople JA, Schleyer PvR, Hehre WJ, Salem LJ (1972) J Am Chem Soc 94:6221
20. Sauers RR (1999) Tetrahedron 55:10013
21. Yamaguchi M, Momose T, Shida T (1990) J Chem Phys 93:4211
22. Brooks PR (1988) Chem Rev 88:407
23. Schatz GC (1990) J Phys Chem 94:6157
24. Bradforth SE, Weaver A, Arnold DW, Metz RB, Neumark DM (1990) J Chem Phys 92:7205